JOURNAL OF GEOPHYSICAL RESEARCH, VOL. 114, B06402, doi:10.1029/2008JB005799, 2009

New insights into the basement structure of the West Siberian Basin from forward and inverse modeling of GRACE satellite gravity data

C. Braitenberg[1] and J. Ebbing[2,3]

Received 13 May 2008; revised 15 February 2009; accepted 17 March 2009; published 3 June 2009.

[1] The oil- and gas-rich West Siberian Basin is underlain by a layer of flood basalts of late Permian-Triassic age that are coeval with the Siberian traps. The extent and thickness of the basalts are unknown, but knowing their thickness is important for discussions on the end-Permian mass extinction because basalt volume constrains estimates of emitted volatiles. We have used GRACE satellite and terrestrial gravity data to study the structure of the crust and basalt distribution. Published seismic sections are used to constrain the sediment isopachs and to estimate a depth-density function. We use published models of crustal thickness and basement depth to reduce the observed gravity field to the basement level. The resulting three-dimensional density model gives information on density anomalies in the lower crust and upper mantle and on the basalt thickness. We identify several rift-graben structures that are presumably filled with basalt. The lower crust below the West Siberian Basin shows considerable density variations, and these variations allow the region to be divided into four major blocks. The eastern part of the basin, toward the Siberian platform, shows an arch-shaped density increase in the lower crust that is accompanied by a linear high-density anomaly at shallower depths. Our work demonstrates the way in which the GRACE-gravity field can be applied to map geological structures like buried rifts and large basins. The same techniques can be used for other large, remote basins such as those in cratonic South America.

Citation: Braitenberg, C., and J. Ebbing (2009), New insights into the basement structure of the West Siberian Basin from forward and inverse modeling of GRACE satellite gravity data, *J. Geophys. Res.*, *114*, B06402, doi:10.1029/2008JB005799.

1. Introduction

[2] The West Siberian Basin, with an areal extent of approximately 3.2×10^6 km^2 (Figure 1), is one of the largest intracratonic basins of the world. The basin is of broad interest because of its high oil and gas potential, as well as its association with the end-Permian mass extinction. In 2004, 7% of the world's oil was produced from the basin, almost entirely from Jurassic and Cretaceous clastic rocks deposited during the post-rift thermal subsidence phase of the basin [*Vyssotski et al.*, 2006]. The potential for undiscovered, conventionally recoverable oil and gas resources is enormous [*Peterson and Clarke*, 1991] and has been assessed to amount to 55.2 billion barrels (1 barrel = 158.9873 liters) of oil, 18.2 trillion cubic meters of gas, and 20.5 billion barrels of natural gas liquids [*Ulmishek*, 2003].

[3] Another important aspect is related to the end-Permian Siberian trap basalts, which are a possible cause of the end-Permian mass extinction [e.g., *Lane*, 2007]. Coeval basalts underlying the basin were recently detected in wells several kilometers deep [*Saunders et al.*, 2005]. This finding considerably increases the total basalt emission at the end-Permian and is an important aspect in discussions of the climate change that lead to the mass extinction. Improved knowledge of crustal structure is the first step toward a realistic estimate of the basalt volume.

[4] The extent of the basin is well defined [e.g., *Vyssotski et al.*, 2006] when considering its limits toward the Urals (west), toward the Siberian platform (east) and toward the Kazakh Highlands (south). However, the northerly termination of the basin and its transition to the Kara Sea, as well as its northeasterly extent (south of the Taimyr Peninsula) are not as well understood. A key to understanding the formation of the basin is to reveal the crustal structure underlying the basin and to constrain sediment thickness.

[5] The aim of our study is to examine the crustal structure and segmentation of the West Siberian Basin on the basis of gravity-field modeling. We aim to differentiate between basement units that can be characterized by differences in crustal structure. Our study makes a new contribution to the understanding of the basin by using a global geopotential model based on GRACE-gravity data [*Tapley et al.*, 2004] and terrestrial data. We use the EIGEN-GL04C model [*Förste et al.*, 2008] that combines satellite-derived data (to half wavelengths of 150 km) with terrestrial data, to give a gravity field with 50 km half wavelength resolution. The satellite-derived data have the advantage of global coverage that is independent of the ruggedness and remoteness of the terrain. Furthermore, by using the satellite data,

[1]Department of Earth Sciences, University of Trieste, Trieste, Italy.
[2]Geological Survey of Norway (NGU), Trondheim, Norway.
[3]Also at Department for Petroleum Technology and Applied Geophysics, NTNU, Trondheim, Norway.

0148-0227/09/2008JB005799$09.00

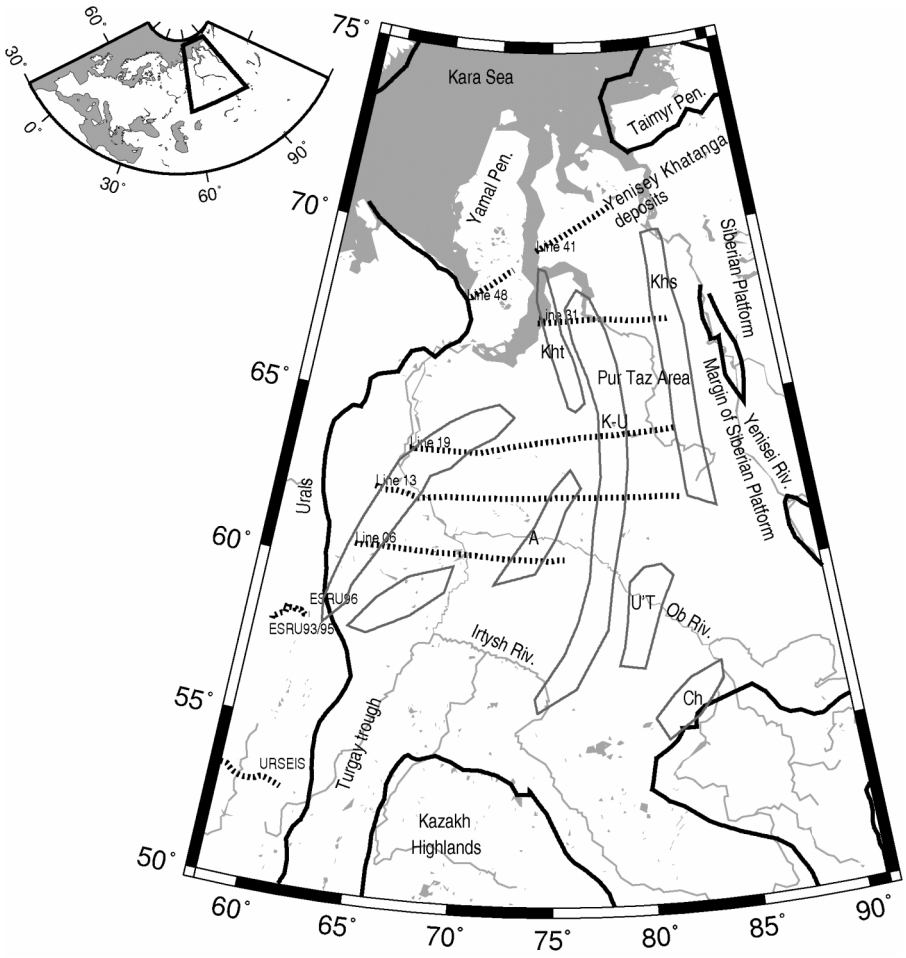

Figure 1. Schematic map showing the main geographic elements of the West Siberia Basin. The map shows the basin outline (bold black line), the 200-m elevation contour (thin black line) and proposed rift-graben structures (polygons are after the study by *Pavlov* [1995]). Names of rift-grabens: K-U, Koltogory-Urengoi; Khs, Khudosei; Kht, Khudottei; A, Agan; U'T, Ust' Tym; Ch, Chuzik. Regional seismic profiles, including the Europrobe seismic reflection profiles across the eastern middle Urals and the west Siberian Basin (ESRU) [*Friberg et al.*, 2000] and the URSEIS 95 seismic experiment [e.g., *Döring and Götze*, 1999], are also shown (stippled black lines). The small insert map shows Europe and Russia (white), with the Mediterranean Sea and Atlantic Ocean (gray). The study area is outlined in black.

we avoid long-wavelength problems in the gravity field that can be introduced when different surface measurement campaigns are combined.

[6] In the following, we first present a forward 3D density model based on well-known crustal structures and compute the model gravity field. Afterward, we compare this field to the observed gravity field and calculate the residual. The second step is to use the residual for a gravity inversion that allows the identification of density anomalies not previously recognized. Finally, we interpret and link our results to the geological setting of the West Siberian Basin.

2. Geological Setting

[7] The basement of the West Siberian Basin consists of Baikalian (Late Precambrian), Caledonian (Cambrian-Silurian) and Variscan (Silurian-Permian) fold systems. A graben system limits the northern part of the basin (Pur-Taz region and Kara Sea). The Siberian flood basalts and intrusives evolved during the Late Permian and the basalts appear to cover the entire basin [*Vyssotski et al.*, 2006]. The age of the flood basalts is about 250 Ma, which is indistinguishable from Siberian trap basalts [*Reichow et al.*, 2002]. The flood basalts within the basin are partly located within the grabens generated by the rifting, but are also present across intervening basement highs, especially in the north [*Surkov*, 2002].

[8] The graben-rift structures have been mapped by *Surkov et al.* [1982, 1993] mainly on the basis of gravity and magnetic fields [*Allen et al.*, 2006]. The main proposed rift grabens are [after *Pavlov*, 1995]: Koltogory-Urengoi, Khudosei, Khudottei, Agan, Ust'Tym and Chuzik (Figure 1). *Pavlov* [1995] questions the fact that the structures are rift grabens, but this has not been confirmed or acknowledged by later authors.

Table 1. Short Summary of the Data, the Data Source, the Native Resolution and the Resulting Resolution During Data Processing

Data Type	Data Source	Native Resolution	Translated Resolution
Gravity	Spherical harmonic expansion of gravity potential, Degree and order ≤ 360[a]	$0.5° \times 0.5°$	55×55 km
DEM	NGDC[b]	30arcsec × 30arcsec	1×1 km
Magnetic field	NGDC[c]	$3' \times 3'$	5.5×5.5 km
Moho	Seismic investigations[d]	unknown	$\sim 100 \times 100$ km
Basement depth	Various compilations[e]	$5' \times 5'$	9×9 km

[a] *Förste et al.* [2008].
[b] 1 km Global Land One-km Base topography, NGDC, Colorado.
[c] *NGDC* [1997].
[d] *Vyssotski et al.* [2006] after *Kovylin* [1985].
[e] Robertson Research (2004), now Fugro-Robertson Ltd.

[9] The volcanic eruption that created the flood basalts was followed by basin-wide subsidence, bringing the basalts down to a depth of 6400 m. It is interesting to note that the flood basalts on the East Siberian platform remained superficial, suggesting different amounts of subsidence between the West Siberian Basin and the East Siberian platform. The Mesozoic to Cenozoic post-volcanic stratigraphic section has been analyzed by *Vyssotski et al.* [2006]. The deepest well in the basin, SG6 (>7 km) [*Pavlenkova et al.*, 2002], does not constrain the lower part of the sediment package, which reaches 15 km depth [*Pavlenkova et al.*, 2002].

[10] *Allen et al.* [2006] present a model for the rift kinematics of the basin and adjacent areas during the Late Permian-Early Triassic that is based on the pattern of magnetic anomalies, existing fault maps and recent geochronological data. The north–south alignment of major grabens is identifiable from magnetic anomalies, as are grabens with NE–SW orientation, the latter implying a component of NW–SE extension. They suggest that West Siberian rifting occurred during regional, right-lateral oblique extension in the Late Permian-Early Triassic. Furthermore, they propose a triple junction in the north of the basin comprising the ENE–WSW trends in the Yenisey-Khatanga Trough, the NW–SE trending magnetic anomalies crossing the Yamal peninsula into the Kara Sea, and the north–south trends of the Koltogory-Urengoi, Khudottei and Khudosei grabens. *Schissel and Smail* [2001] attribute the triple junction to the impact of a mantle plume. Consistent with this idea would be the observation that the greatest post-rift subsidence and sedimentation has taken place in this part of the basin [*Peterson and Clarke*, 1991] and that the area has been described as the focus of basaltic magmatism [*Surkov*, 2002].

[11] Views critical of the existence of a mantle plume [e.g., *Czamanske et al.*, 1998] argue that, unlike many other flood basalt provinces, there is no obvious succeeding plume "trail" leading to a presently active hot spot. It is unclear, therefore, whether any form of mantle hot spot persisted after the formation of the traps. *Saunders et al.* [2005] come to the conclusion that uplift of the northern part of the nascent West Siberian Basin began during the Permian and was perhaps accompanied by rifting. Little or no uplift is predicted for the Siberian Craton. Furthermore, they suggest that the main site of magma generation was located primarily in the northern basin (Khudosei and Urengoi rifts) and that the magma source was common to the flood basalts on the Siberian Craton and on the West Siberian Basin. The magma traveled onto the craton either across the land surface and/or through the crust as dykes or sills. *Saunders et al.* [2005] propose that following the main period of continental flood basalt formation, the locus of magmatism migrated northward to what is now the Taimyr Peninsula, and thence onto the Barents Shelf. The West Siberian Basin presumably then underwent thermal subsidence [*Saunders et al.*, 2005]. We will show later that crustal loading may also have contributed to the subsidence.

3. Databases Used in the Study

[12] Our study requires consideration of several data sets (see Table 1) that have been collected from different sources. The data are graphed and discussed in the following.

3.1. Gravity and DEM

[13] Our analysis relies on regional data because detailed local data are not readily available. A digital elevation model (DEM) is indispensable for correcting gravity data for the effects of topography. For this purpose, we use the 1-km GLOBE (Global Land One-km Base Elevation) grid (Figure 2a) released by the National Geophysical Data Centre in Boulder, Colorado (NGDC). Gravity-field data are available at a spatial resolution of $0.5° \times 0.5°$ from global geopotential models that combine satellite and surface gravity measurements. We have used the EIGEN-GL04C model (Figure 2b) that includes spherical harmonic coefficients up to degree and order 360 [*Förste et al.*, 2008] and is based on the GRACE (Gravity Recovery and Climate Experiment) satellite mission. In the harmonic expansion, the coefficients up to degree and order 70 are derived purely from satellite measurements, degrees 70 to 116 have been obtained by combining the satellite gravity data with surface data, and the higher orders are from surface gravity measurements. The surface gravity measurements include gravity data from altimetry and ships over the oceans and airborne or terrestrial measurements over continental areas. In general, the lower-order harmonics of EIGEN-GL04C are a substantial improvement on the earlier EGM96 model. This is important because these lower-order harmonics are closely related to deep subsurface structures like the Moho and the deeper interior of the Earth [see, e.g., *Shin et al.*, 2007].

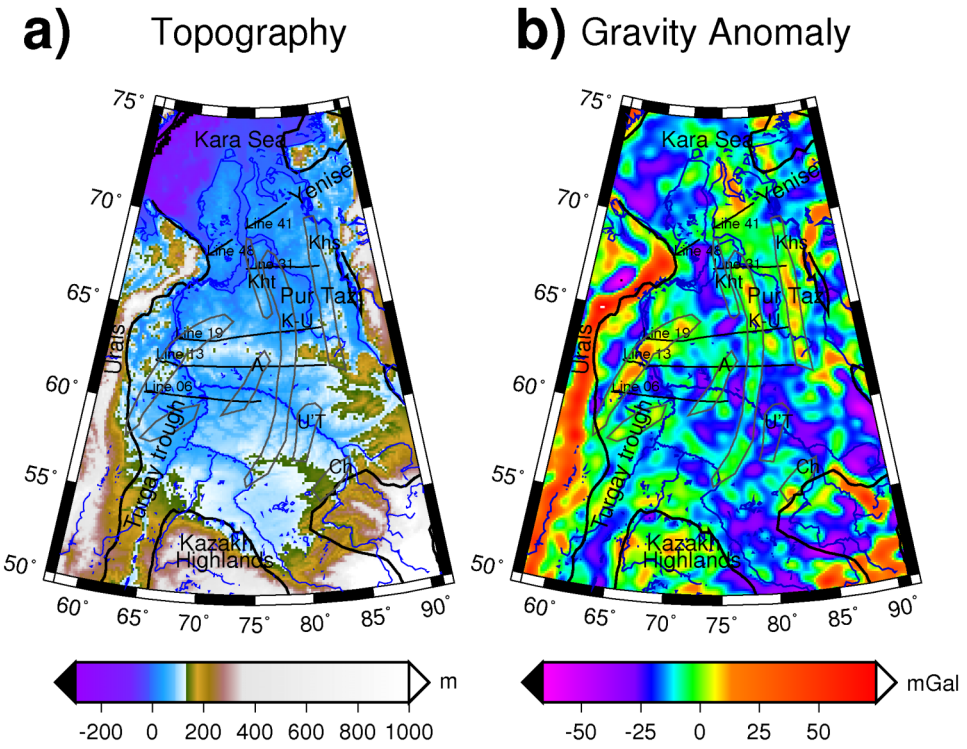

Figure 2. (a) Topography of the West Siberian Basin area. (b) Free-air gravity anomaly (mGal = 10^{-5} m/s^2) for the West Siberian Basin area from the EIGEN-GL04C global geopotential model [*Förste et al.*, 2008]. The maps are overlain by the coastline and major rivers (blue), the basin outline (bold black), and the seismic lines and rifts (as in Figure 1).

[14] The combined satellite and terrestrial gravity fields must be corrected for the topography in order to obtain the Bouguer anomaly (Figure 3a). We use the DEM mentioned above for the near-field correction (<10 km from each grid point) and have computed a coarse grid (0.1° resolution) from the DEM for the far-field correction (10–167 km). Calculations are computed on a spherical Earth following the procedure proposed by *Forsberg* [1984] and using the GRAVSOFT package [*Tscherning et al.*, 1992]. Standard densities were used for the Bouguer correction, which were 2670 kg/m^3 and 1030 kg/m^3 for the terrain and water density, respectively.

[15] The mean free-air gravity anomaly (Figure 2b) over the central part of the West Siberian Basin varies between −5 and −25 mGal. In the northern part of the basin, three linear highs are evident. These highs are associated with graben structures [*Allen et al.*, 2006; *Peterson and Clarke*, 1991; *Pavlov*, 1995], in particular the Khudottei (west), Koltogory Urengoi (central) and Khudosei (east) graben. The basin itself is bounded by positive free-air gravity anomalies: the Urals (+60 mGal), the Kazakh highlands to the South (+20 mGal) and the East Siberian platform to the east. The Bouguer gravity field (Figure 3a) displays very similar features to those evident in the free-air gravity anomaly over the West Siberian Basin: the basin has generally negative Bouguer anomalies that oscillate around −15 mGal.

3.2. Magnetic Data

[16] Magnetic data for the West Siberian Basin are available from the National Geophysical Data Center [*NGDC*, 1997]. These data are based on digitized map sheets at 1:2.5 million scale and show the residual magnetic intensity over the landmass of the former U.S.S.R. NGDC converted these data to a latitude/longitude projection and regridded them to a 3 minute grid to allow the interpretation of regional anomalies. The procedure used to retrieve the magnetic anomalies does not allow the interpretation of local anomalies and, for this reason, we only use the magnetic data for qualitative comparison with the results of our forward and inverse modeling of the density structure in the study area.

[17] The magnetic anomaly map (Figure 3b) has linear features that are similar to the lineations evident in the free-air and the Bouguer gravity maps. The Khudottei (west), Koltogory Urengoi (central) and Khudosei (east) graben systems are associated with pronounced linear magnetic highs. In the southern part of the basin, the magnetic anomalies are of shorter wavelength and do not seem to correlate with the graben system. Instead, the anomalies are probably related to shallow crustal sources.

3.3. Moho Depth

[18] The Moho depth (Figure 4a) has been digitized from *Vyssotski et al.* [2006], who relied on the results of *Kovylin* [1985]. A very similar Moho depth map, based on the study by *Karus et al.* [1984], is presented by *Artyushkov and Baer* [1986]. The Moho under the basin is between 36 and 40 km deep and deepens to 48 km westward below the Urals and eastward below the East Siberia platform. Shallow Moho depths are found in the Kara Sea. Published work does not allow uncertainties in Moho depth to be estimated.

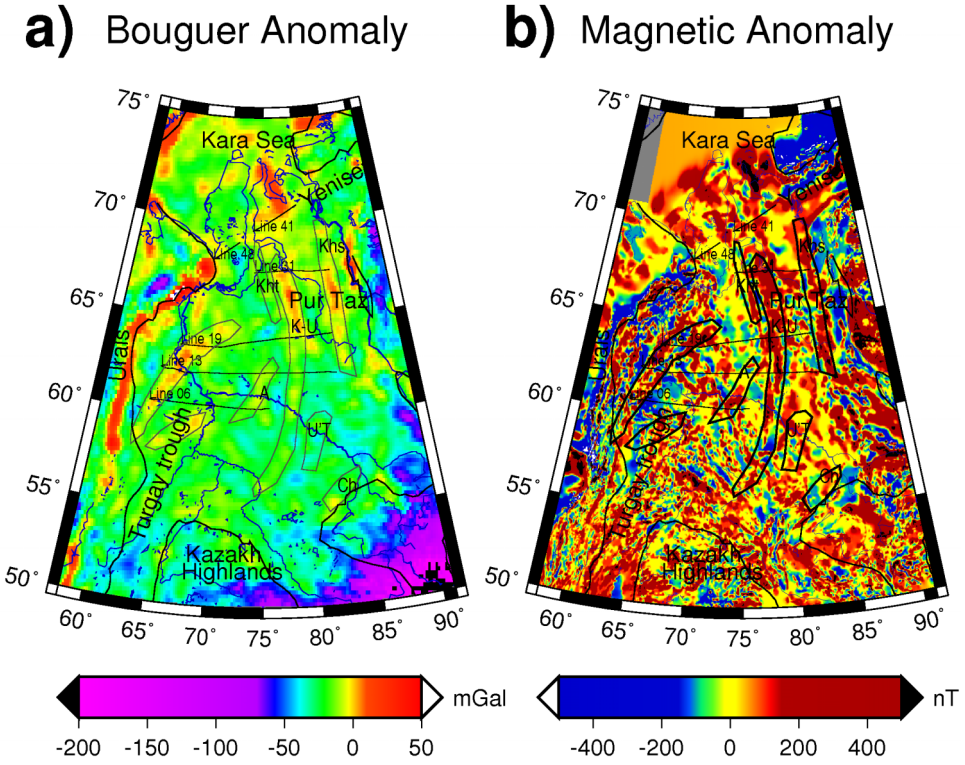

Figure 3. (a) Bouguer gravity anomaly (mGal) for the West Siberian Basin area derived from the free-air anomalies shown in Figure 2b. (b) Magnetic anomaly field for the West Siberian basin [*National Geophysical Data Center*, 1997]. The maps are overlain by the coastline and major rivers (blue), the basin outline (bold black), and the seismic lines and rifts (as in Figure 1).

3.4. Basement Depth and Sediment Layer

[19] We use a sediment thickness model that is based on information extracted from a Statoil-Hydro database. This was compiled in 2004 by Robertson Research (now Fugro-Robertson Ltd) based on Robertson Research internal data (basement outcrops, sediment thickness contours), the Exxon global sediment thickness map released to AAPG in 1991, and publications such as *Peterson and Clarke* [1991] who updated data from *Aleinikov et al.* [1980]. The map was digitized with a spatial resolution of $5' \times 5'$ over the entire West Siberian Basin (Figure 4b). The sediment thickness model describes the entire sediment package, so it includes the pre- and post-late Permian/Triassic basalt layer. The maximum sediment thickness reaches more than 15 km (e.g., at 77.85°E, 67.33°N). The sediments extend continuously eastward into the Yenisey-Khatanga deposits. The southern half of the basin is wider, but the deepest part (thickness >5000 m) is elongated and relatively narrow, indicating smaller characteristic wavelengths. In the southern part of the basin, we find a succession of linear, NNW–SSE-oriented structures in the basement that are deeper than the areas bording them. These correlate with the magnetic anomalies.

3.5. Resolution Analysis

[20] For spherical harmonic coefficients greater than degree and order 130, the EIGEN-GL04C gravity field has an accuracy of about 0.5 mGal [*Förste et al.*, 2008]. The accuracy is better for lower degree and order. Assuming a source approximated by a boundary w(r) separating two layers with density contrast $d\rho$, the gravity field, to first approximation, is given by the first term of the Parker series expansion [*Blakely*, 1995]. Using a value for the gravity anomaly of 0.5 mGal at a wavelength λ and given the average depth at which the boundary is located and the density contrast across the boundary $d\rho$, we can calculate the oscillation amplitude that the boundary must have in order to generate a 0.5 mGal signal. The oscillation amplitude gives the sensitivity of the gravity field, as it represents the smallest oscillation amplitude of the boundary that can be detected by the gravity field. In Figure 4c, the oscillation amplitude is plotted for different values of the average reference depth, assuming a density contrast of 500 kg/m^3. The shallower the mass boundary, the smaller is the amplitude that can be detected. The density contrast acts as a linear scaling factor and a decrease in the density contrast requires a proportional increase in the boundary amplitude to produce the same signal. The smaller the wavelength the greater is the required boundary amplitude in order for it to be detected. At the level of the basalt layer (5 km depth), the resolution of the basalt thickness is near to 100 m at wavelengths of 20 km and greater. At Moho level (40 km depth) the amplitude of the boundary is resolved at the kilometer level at wavelengths of 80 km and greater.

4. Two-Way Traveltime to Depth Conversion

[21] Our study requires an estimate of the gravity effect produced by the sediments, for which information on the

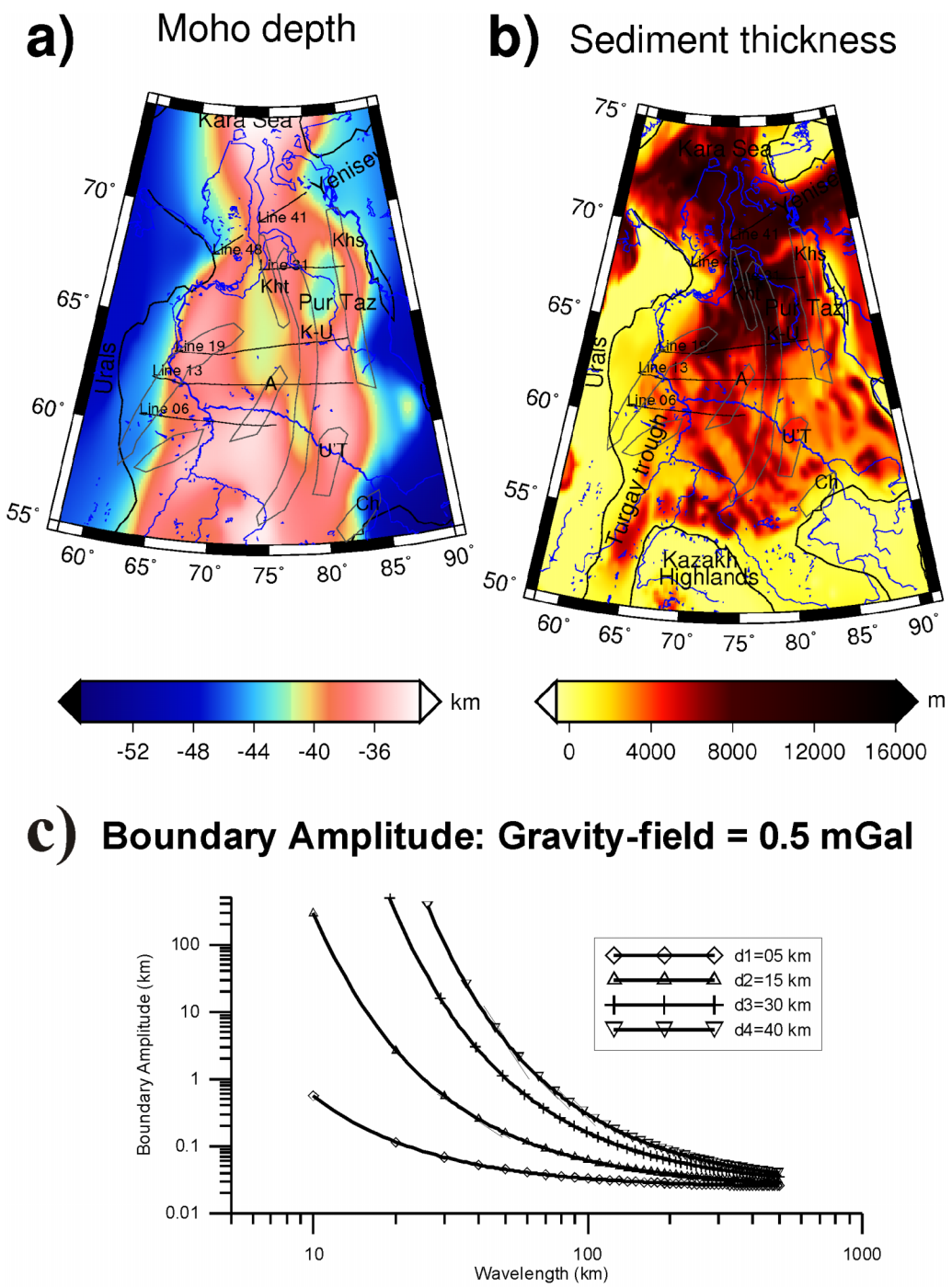

Figure 4. (a) Moho depth for the West Siberian Basin area based on the study by *Kovylin* [1985] (digitized from the study by *Vyssotski et al.* [2006]). (b) Sediment thickness map. In both maps, black lines show regional seismic profiles. The coastline and rivers are shown by blue lines. (c) Plot showing the sensitivity of the observed gravity field to the amplitude of intracrustal boundary oscillations at different anomaly wavelengths and for a detection limit of 0.5 mGal (the approximate error in the EIGEN-GL04C data at degree and order 130).

sediment density is needed. We infer the sediment densities from a relationship between horizon depth and two-way traveltime (TWT). This relationship was obtained from the sedimentary horizons in seismic sections presented by *Vyssotski et al.* [2006]. The TWT-depth relationship is also used to estimate the depth of the basalt layer, where it has been identified in the seismic sections.

[22] A series of seismic profiles crossing the West Siberian Basin is presented in the study by *Vyssotski et al.* [2006]. They report the calibrated TWT (two-way traveltime) for some horizons, for some of the profiles and for the

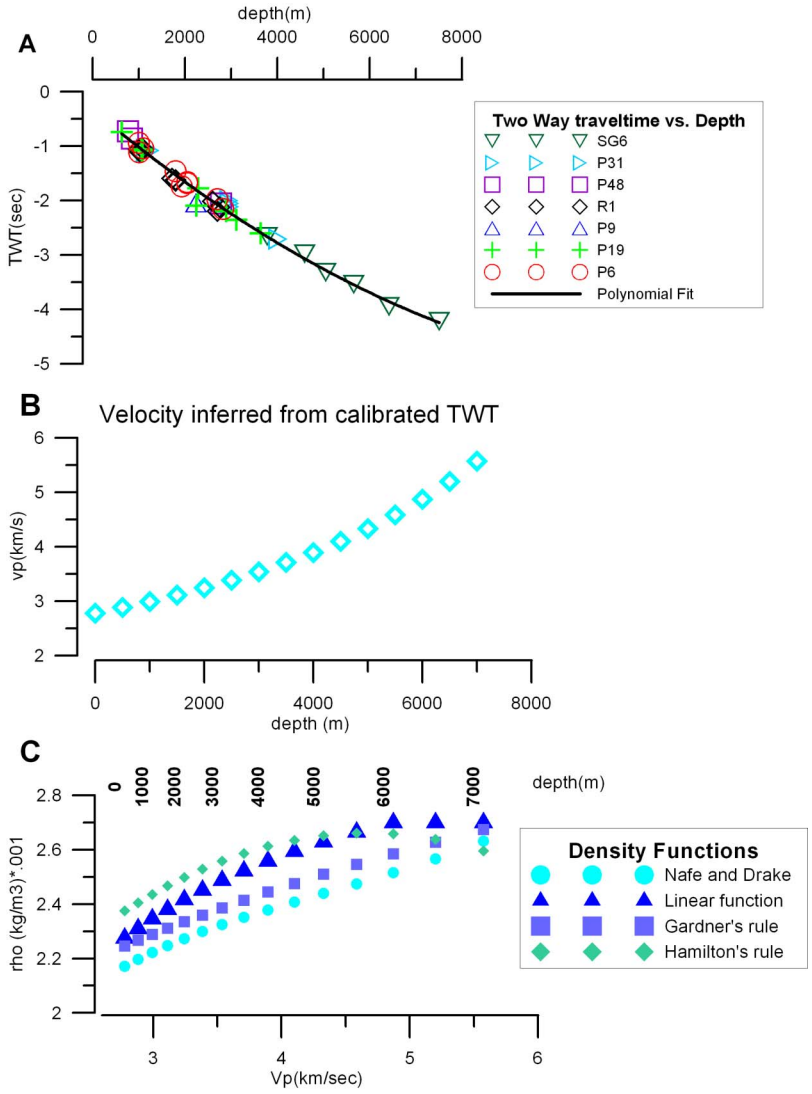

Figure 5. (a) Two-way traveltime (TWT) versus depth for a selection of seismic profiles and for the deep well SG6 [*Vyssotski et al.*, 2006]. (b) Velocity of sediments as a function of depth derived from an analysis of the TWT data. (c) Comparison of the depth-dependent linear density increase. Different equations were used for calculating the relationship between density and velocity (Nafe-Drake: *Ludwig et al.* [1970], *Jones* [1999]; Gardner's rule: *Gardner et al.* [1974]; and Hamilton's relationship: *Larsen et al.* [1994]).

deep well SG6. In Figure 5a, the TWT (in seconds) is plotted against the depth (d in m) for the available data. Fitting the observed data with a polynomial function results in the following relationship:

$$TWT = 0.33 + 0.00072d - 2.58 \times 10^{-8} d^2 \qquad (1)$$

with d the depth.

[23] The second step is to convert the TWT to depth by using velocities of the strata. Assuming near-vertical reflections, the TWT for a horizon with depth d can be estimated by:

$$TWT = 2 \int_0^d \frac{1}{v(z)} dz \qquad (2)$$

where $v(z)$ is the velocity as a function of depth. By matching equation (2) with the polynomial approximation of the TWT versus depth function (equation (1)), we find that the slowness (inverse of velocity) is a linear function of depth:

$$s(z) = \beta + \gamma z \qquad (3)$$

where $\beta = 3.6 \times 10^{-4}$, $\gamma = -2.58 \times 10^{-8}$.

[24] For the velocity (m/s) this translates to:

$$v(z) = 2780 \frac{1}{1 - 0.72 \times 10^{-4} z} \qquad (4)$$

with z the depth (m).

[25] At 1000 m depth, equation (4) gives a velocity of 2996 m/s, increasing to 5605 m/s at a depth of 7000 m. By applying empirical velocity-density relationships, the depth dependency of the velocity also allows sediment densities to be estimated. As uncertainties exist regarding the velocity-density relationship, we adopt three relationships: the well known Nafe-Drake curve [e.g., *Jones*, 1999], Gardner's rule [*Gardner et al.*, 1974], and Hamilton's relationship [*Larsen et al.*, 1994]. All three are valid for sediments [*Brocher*, 2005]. The results are shown in Figure 5c, where the density is given as a function of the velocities corresponding to depths ranging from the surface to 7000 m. We find that a linear density-depth variation model has a deviation of up to 100 kg/m^3 from Hamilton's relationship and gives consistently higher densities than do Gardner's rule and the Nafe-Drake empirical relationship. Using the Nafe-Drake or Gardner relationship will increase the gravity effect of the sediments. Therefore our approach, as outlined below, can be considered to provide a minimum estimate of the gravity effect of the sediments.

5. Forward Modeling of the Crustal Density Structure

[26] In this section, we discuss the observed gravity fields and determine to what extent the observations agree with present knowledge of the crust and lithosphere. The results lead to the recognition of different terranes that constitute the West Siberian Basin. All calculations were made using the Lithoflex software (www.lithoflex.org; [*Braitenberg et al.*, 2007]).

5.1. Gravity Effect of Sedimentary Rocks

[27] The Bouguer anomaly represents the gravity field produced by the crustal column, excluding the topography. By subtracting the gravity effect of the sediment layers, we can enhance the gravity effect of underlying structures. We use the entire sediment package containing both post- and pre-basalt flow layers and the sediment thickness map presented in Figure 4b. For modeling, we use the linear density variation explained in section 4. The density increases linearly from 2275 kg/m^3 at the surface to 2700 kg/m^3 at a depth of 6 km, and remains constant at 2700 kg/m^3 for greater depths (Figure 5c). The calculations were made by dissecting the basin into layers of 10 m thickness and calculating the gravity field of each layer [*Braitenberg et al.*, 2006; *Blakely*, 1995]. The resulting gravity effect of the sediments is near to −50 mGal over large parts of the basin, with a maximum of −70 mGal (Figure 6a). It follows that the sediment correction shifts the Bouguer anomalies toward more positive values.

5.2. Gravity Effect of Crustal Thickness

[28] The next step in stripping the known masses to gain insights into the "unknown" crustal structure is to reduce the gravity field for the effect of crustal thickness variations. We calculate the gravity effect of the crustal thickness variations using the Moho depth as published in the study by *Vyssotsky et al.* [2006], a typical value of 350 kg/m^3 for the density contrast at the Moho, and a normal crustal thickness of 35 km (as used in standard Earth models like PREM [*Dziewonski and Anderson*, 1981]). Calculations were made with the Parker series expansion for an undulating boundary [*Blakely*, 1995]. The resulting gravity effect varies between −180 mGal and −30 mGal (Figure 6b). Using a different density contrast will linearly affect the calculated gravity field: a 10% increase in the density contrast results in a 10% increase in the gravity values.

[29] The resulting residual field (Figure 6c) represents the Bouguer field stripped of the gravity effect of sediments and crustal thickness variations. It is more positive than the initial Bouguer anomaly because both the sediments and the Moho, which is systematically deeper than the reference depth, represent a mass deficit. The residual field has its maximum values along the Urals. In the northern Urals, the linear gravity high is offset eastward into the basin. High values are also evident in the northern part of the basin where sediment thickness is greatest.

[30] It is interesting to note that toward the Urals, crustal thickening (Figure 4a) varies independently of topography. Increased crustal thickness exists well within the basin to the east of the topographic increase related to the Urals. This suggests that the Moho variations are related to buried features rather than the transition from basin to orogen.

5.3. Gravity Effect of the Basalt Layer

[31] In addition to the information about sedimentary and crustal thickness, we can also consider the information about the presence of basalts in the West Siberian Basin. The recovery of basalt from boreholes demonstrates that basalt extends over large parts of the West Siberian Basin. However, their areal extent and thickness are only roughly known. *Vyssotski et al.* [2006] report a minimum and maximum areal extent that differs by 100%. In addition, the thickness of the basalt layer is poorly known and large uncertainties exist in the rift grabens. To estimate the minimum contribution of the basalt layer to the gravity field, we interpolate the basalt boundaries from the line drawings of the regional seismic profiles in the study by *Vyssotski et al.* [2006].

[32] We interpolate the acoustic basement, which corresponds to the top Permian and the top basalt, onto a regular grid with a 15 km interval. The model we obtain for the top basalt is affected by the relatively short profiles and the large spacing between profiles. This does not allow a good 3D representation of the basalt layer and our estimate is only a crude approximation that is possibly subject to major, unmodeled changes in basalt extent and depth. In Figure 7a, the top of the interpolated basalt layer is shown. The seismic profiles suggest that the basalt layer appears to be less than 0.6 km thick, but this thickness estimate does not include the basalt in the rift grabens. The greatest basalt thickness is found in the north–east (Pur Taz area; 77°E, 66°N) along profiles 27 and 31. Basalts have a characteristic density of 2700–3000 kg/m^3 [*Mussett and Khan*, 2000] and, with a density contrast of 300 kg/m^3 to the surrounding bedrock, this basalt layer produces a gravity signal that amounts to 6 mGal at most (Figure 7b). As the uncertainties are rather large, we also calculated the gravity effect of a basalt layer, resting on the acoustic basement, with a constant thickness

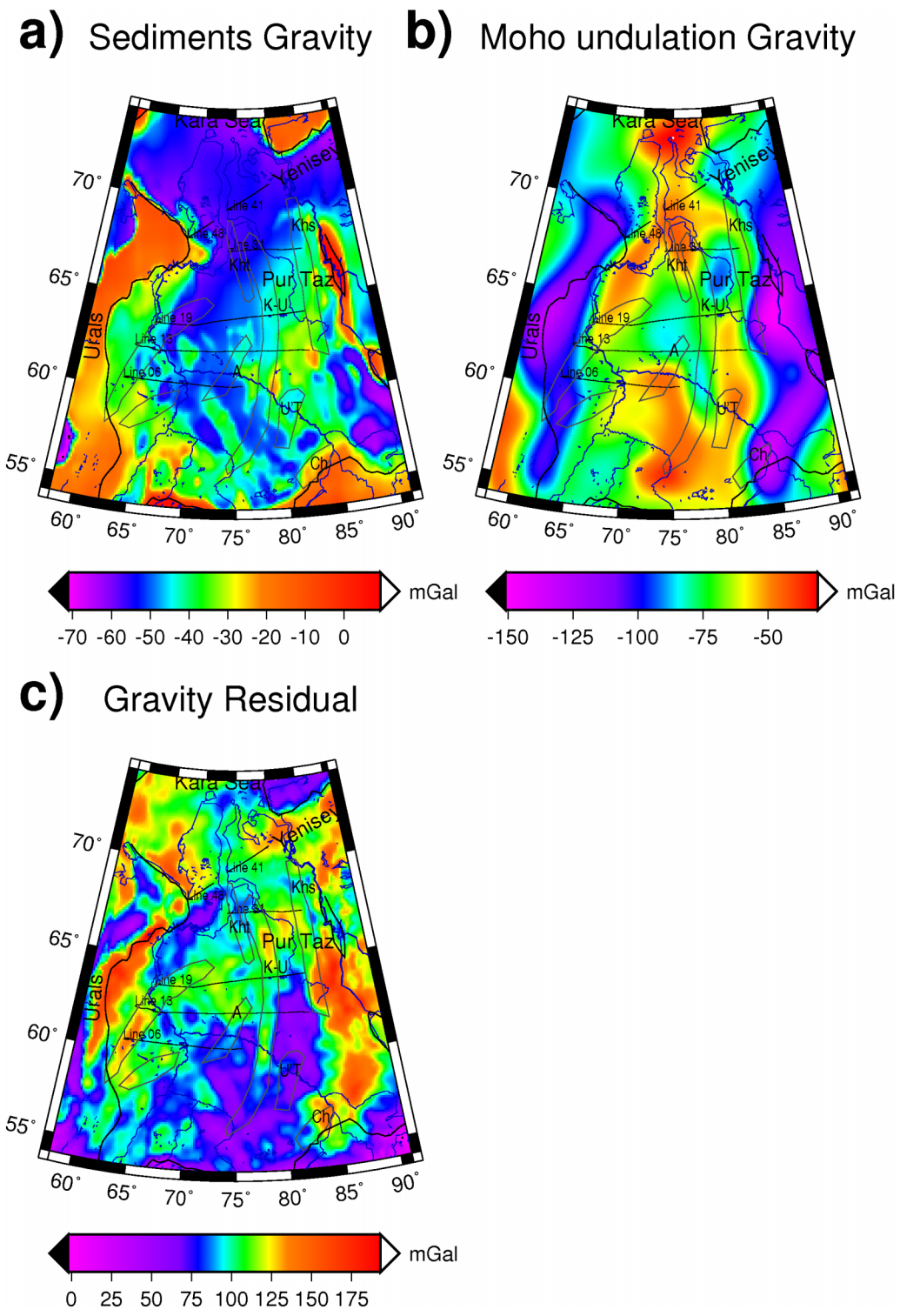

Figure 6. (a) Gravity effect of sediments derived from the thicknesses shown in Figure 4b. (b) Gravity effect caused by the density contrast at the Moho. Reference depth: 35 km; density contrast: 350 kg/m^3. (c) Gravity residual after correcting for topography, sediments and crustal thickness variations. Maps also show the coastline and major rivers (blue), basin outline (bold black), seismic lines and rifts (as in Figure 1).

of 1 and 2 km, The calculations were made using the Parker series expansion [*Blakely*, 1995]. The gravity signal of these layers has a nearly constant value of 12 and 25 mGal, respectively. The uncertainties associated with the calculated gravity effect of the basalt layer are so large that removing this effect from the observed gravity is not useful at this stage. Instead, we attempted to gain more insights into the basalt thickness by inverting the gravity field. However, the

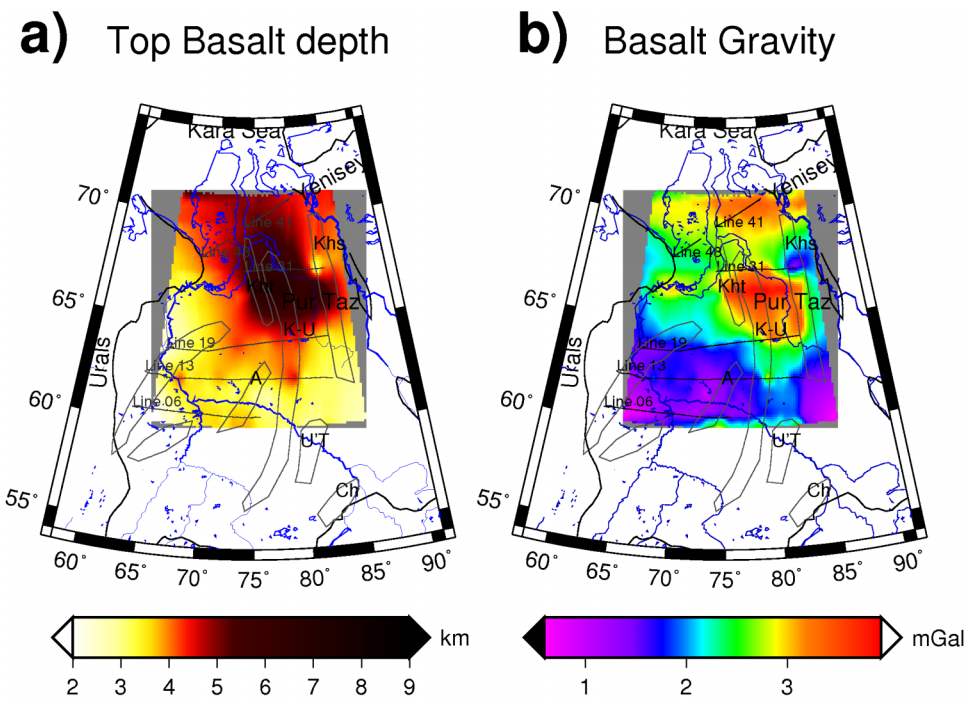

Figure 7. (a) Map of modeled depth to the top of the basalt layer; the depth is only constrained along the profiles shown in black. (b) Order-of-magnitude estimate of the gravity signal produced by the basalt layer.

forward estimates of the basalt gravity effect are useful as a means to evaluate the uncertainties in our results.

6. Inverse Modeling

[33] So far, the residual gravity field corrected for the effect of sediments and crustal thickness variations leads to a positive gravity residual (Figure 6c) that cannot be explained by the gravity effect of the end-Permian basalts (Figure 7b). In order to distinguish the features contained in the residual field, we use a cosine taper filter to separate the field into components with wavelengths longer (Figure 8a) and shorter (Figure 8c) than 270 km. The appropriate cut-off wavelength is chosen such that the average high-pass filtered gravity residual is equal to zero. This criterion assumes that superficial mass anomalies are distributed randomly between positive and negative anomalies, so the average field will approach zero. We have tested a range of cut-off wavelengths between 30 km and 370 km and find that an appropriate wavelength that separates the superficial from the deeper-seated masses is 270 km.

[34] The low-pass filtered residual (Figure 8a) shows entirely positive values that range between 50 and 150 mGal. These high residual values indicate that the sediment correction and the correction for crustal thickness are not sufficient to explain the observations, which implies that mass inhomogeneities other than sediment thickness variations and crustal thickening are present. Two symmetrically opposed positive anomalies are evident and they delineate the basin along its eastern and western border. The anomaly to the east borders the transition to the Siberian platform (82–90°E), while the anomaly to the west borders the Urals (60–65°E). The basin itself is dissected by a NE–SW trending relative gravity high (extending northeastward from 65°E, 58°N) that is about 50 mGal higher than the adjoining part of the basin. This positive gravity zone is coincident with the areas of the inferred graben and rift structures, but covers a broader region. In the northern part of the basin, the Yenissey-Khatanga trough (85°E, 70°N) and the transition to the Kara Sea are also associated with high gravity residuals.

[35] The high-pass filtered residual (Figure 8c) highlights several features in the basin. An almost symmetric gravity high coincides with the eastern (along 85°E) and western (along 62°E, bending eastward north of 64°N) borders of the basin. The western high is partly centered on the Urals and partly extends eastward into the basin. The Pur Taz area (80°E, 67°N) is a general high from which a linear high protrudes southward (along 77°E). This linear high is associated with the Koltogory-Urengoi and Khudosei grabens. An additional linear positive anomaly, presumably tied to the graben, is evident to the east of the Urals (extending northeast from 64°E, 59°N). This could be the westward extension of the Agan graben [*Pavlov*, 1995]. The Kara Sea shows small residual anomalies, an indication that the crustal thickness variations and the sediments are sufficient to explain the observed gravity field there. The Yenisey-Khatanga Trough is characterized by positive residual anomalies.

[36] In the next step, we tried to associate the filtered gravity anomalies with features in the upper and lower crust. For this purpose, we inverted the low-pass filtered residual gravity field to a layer with variable density located just above the Moho by applying an iterative inversion procedure. The layer is assumed to have a thickness of 20 km and the resulting lower-crustal density contrasts range between 80 kg/m^3 and 230 kg/m^3 (Figure 8b). From the available seismic profiles, we have no constraints on the thickness of

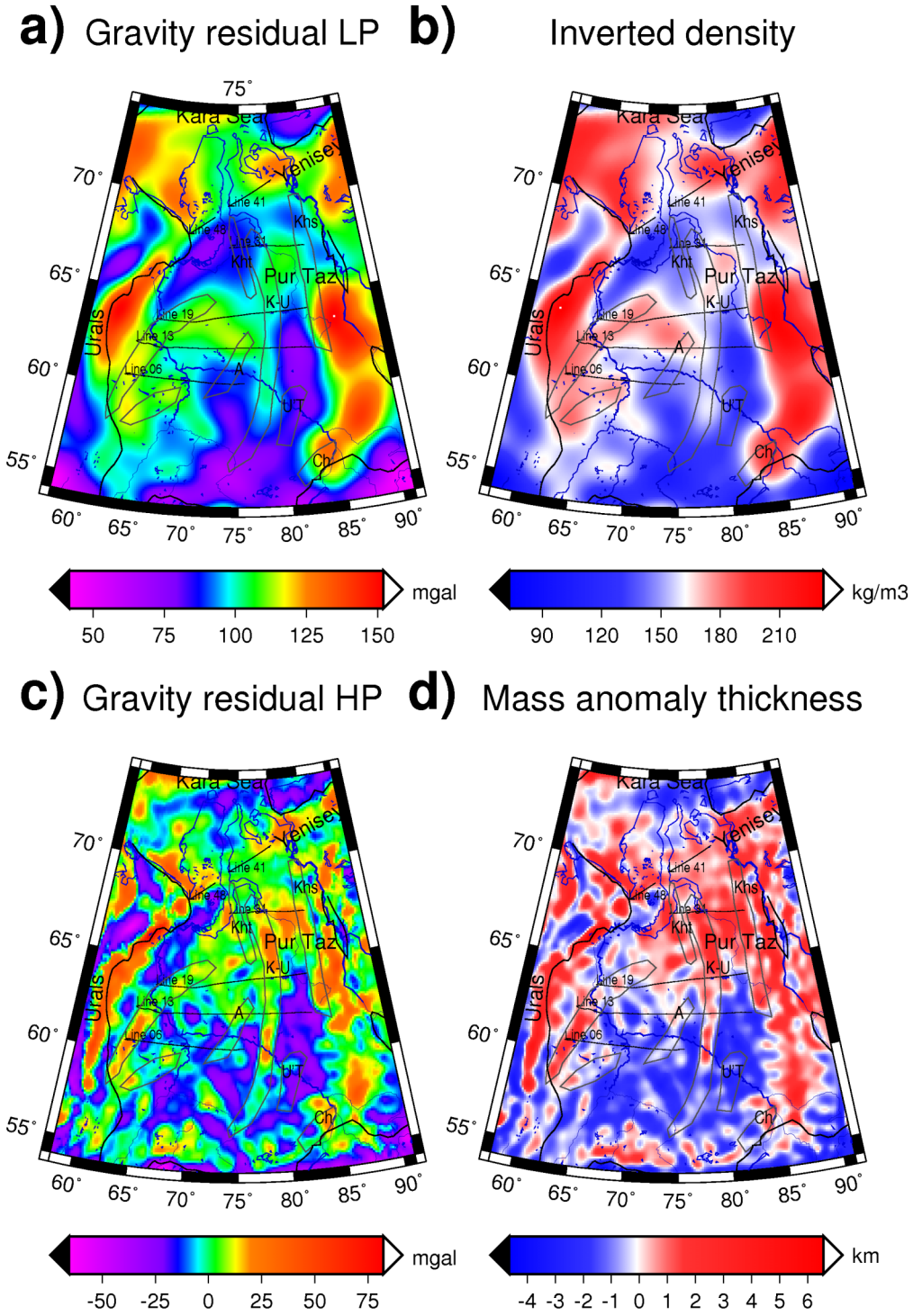

Figure 8. (a) Low-pass filtered gravity residual based on the Bouguer anomaly corrected for sediments and crustal thickness variations (Figure 6c). (b) Density variations in the lower crust needed to explain the long-wavelength part of the residual gravity field. (c) High-pass filtered gravity residual based on the Bouguer anomaly corrected for sediments and crustal thickness variations (Figure 6c). (d) Thickness of possible upper-crustal basalt layer obtained by inverting the high-pass filtered residual gravity field. The masses are assumed to have a density contrast of ±300 kg/m^3 to the surrounding basement depending on whether they are above or below a reference depth of 5 km, respectively. See text for details.

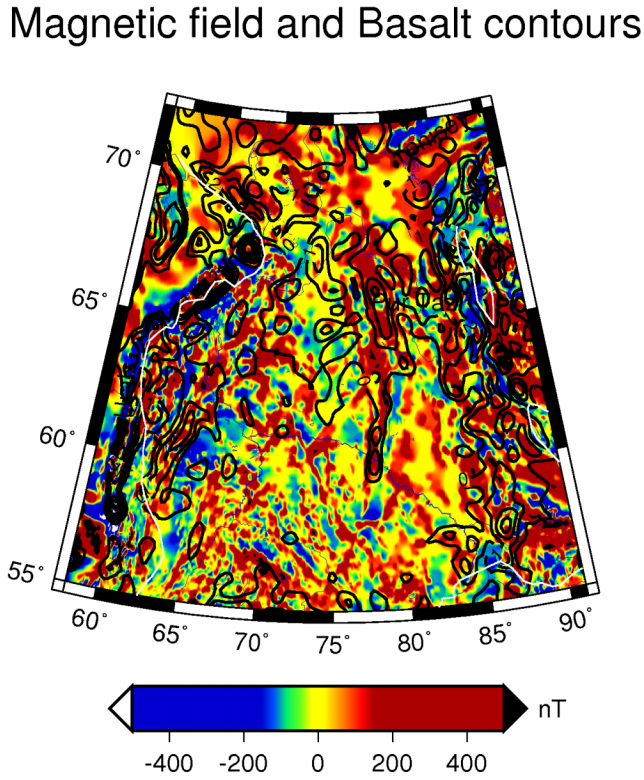

Figure 9. Magnetic anomaly map (nT) and contours of the inverted thickness of the basalt layer from Figure 8d (contour interval: 1 km).

the increased density layer, which could also have a variable thickness. The thickness acts as a scaling factor on the inverted density: a thinner layer would lead to a proportionally higher density, whereas a thicker layer would lead to a lower density than is shown in Figure 8b.

[37] The most prominent density increase is found below the Urals and along the southeastern margin of the basin, flanking the transition to the Siberian craton. The Pur Taz region is also characterized by a moderate density increase that extends southward and south–westward. The south–western density increase is found over a broad area. The area east of the Urals is associated with increased density that coincides with the western ends of the seismic profiles 19, 13 and 06. Another area with increased density is found along the Yenisey Khatanga trough.

[38] The high-pass filtered gravity residual has several linear features that are likely to correlate with inferred graben structures [e.g., *Allen et al.*, 2006]. An interesting question is to what extent the graben structures are filled with volcanic and sedimentary rocks. The volcanic rocks should contribute to a positive, the sedimentary rocks to a negative gravity signal. We tentatively interpret the residual anomalies with positive or negative masses located below and above a reference level, respectively. Using this approach, we invert the residual gravity of Figure 8c to give the layer thickness shown in Figure 8d. The inversion was made using a reference level of 5 km and a density contrast of ±300 kg/m^3. A positive anomaly is inverted using a positive density contrast with the mass located below the reference level and a negative anomaly is associated with a negative density contrast with the mass being above the reference level. The masses have varying thickness. In this case, the positive masses can be interpreted as a magmatic body (basalts), whereas the negative masses point to the presence of low-density material (e.g., from a deeper basin or a lower compaction rate than assumed in our model).

[39] The comparison between the magnetic anomaly and the inverted upper-crustal structures shows that in general there is a good correlation between the upper-crustal mass surplus and positive magnetic anomalies (Figure 9). Most of the linear mass structures are associated with high-amplitude magnetic anomalies. In contrast, the southern part of the West Siberian Basin is associated with negative mass anomalies in the upper crust. Here the magnetic anomaly map mostly shows less continuous, short-wavelength anomalies. These can be associated with magmatic intrusions in the upper crust, but these intrusions must have significantly less volume than in the north.

7. Discussion

[40] In the course of this study, we have calculated the gravity effect of all known masses (crustal thickness variations, sediments and, crudely, the basalt layer) and have shown that a considerable residual remains. The high-pass filtered gravity residual has several linear features that are very likely to correlate with inferred graben structures [e.g., *Allen et al.*, 2006].

[41] We can draw some useful conclusions from the short-wavelength residual gravity field (wavelengths less than 270 km; Figure 8c). Linear gravity highs can be identified and these highs correlate with highs in the magnetic anomaly. The structures associated with these highs are interpreted to be linear positive masses related to rift-graben units [*Pavlov*, 1995; *Allen et al.*, 2006]. The most prominent are the Koltogory-Urengoi, the Khudottei, and the Khudosei grabens. Also of interest is the NE–SW trending rift-graben structure in the western-central part of the basin. This structure produces a prominent gravity signal and lies in the area of increased lower-crustal density.

[42] Another well-developed structure extends for a length of over 1500 km along the eastern margin of the basin. It partly runs along the Yenisey river, so we refer to it as the Yenisey anomaly. It overlaps and crosses the eastern high-density arch evident in Figure 8b. The Yenisey anomaly is located east of the Khudosei rift, an observation already made by *Allen et al.* [2006] from the interpretation of magnetic data. At its northern end (85°E, 70°N), the Khudosei anomaly bends eastward into the Yenisey-Khatanga trough. Across the trough, we find a symmetrically located linear gravity high (85°E, 72°N). Comparison with mapped geology suggests that the Yenisey anomaly is associated with an ancient fold belt, the Yenisey Fold system [*Peterson and Clarke*, 1991], that formed toward the end of the Precambrian during the Baykalian orogeny.

[43] We have also demonstrated the existence of large, long-wavelength residual anomalies (Figure 8a), up to roughly 150 mGal, that suggest the presence of lower-crustal masses with increased density. The high-density basalts evident in seismic data [*Vyssotski et al.*, 2006] cannot explain the entire gravity signal. We estimate the

contribution from seismically imaged basalt to be less than 25 mGal (section 5.3), but acknowledge that the 2 km maximum thickness used to make this estimate is probably exaggerated. This estimate of the basalt gravity effect does not include basalt in the rift grabens where they are probably thicker, but contribute only to the short-wavelength gravity anomalies. Seismic investigations give some indication that the mantle below the West Siberian crust has relatively low velocities [*Morozova et al.*, 1999], which is not consistent with a density surplus in the mantle. Hence we propose that these masses are located both in the lower and upper crust.

[44] When we consider longer wavelength anomalies and interpret these as being caused by density variations in the lower crust, we infer segmentation of the basement. This segmentation is most clearly evidenced by an arch-shaped density increase along most of the eastern and western (along the Urals) borders of the basin. As mentioned above, the eastern structure could represent the Yenisey fold belt, or Baykalides, a unit that is included in the generalized tectonic map of *Sengor and Natal'in* [1996], displayed in the study by *Vyssotski et al.* [2006] and discussed in the study by *Peterson and Clarke* [1991]. The Urals have been studied in detail by the URSEIS (south) and the EUROPROBE seismic investigations of the middle Urals [*Friberg et al.*, 2000]. The gravity high of the Urals is well known and has previously been explained by the combined effect of mafic-ultramafic rocks exposed on the surface and high-density rocks at Moho level [*Döring et al.*, 1997; *Döring and Götze*, 1999] or by the gravity effect of relict, southwest-dipping subduction [*Friberg et al.*, 2000]. The lower-crustal density variation in the basin allows the identification of a southern and mid-western segment (slightly increased density), a middle segment that includes the Pur Taz area (moderately high density), and a northern segment (moderately high density).

[45] The graben structures that we identified in the high-pass filtered gravity residual and the magnetic anomaly fields only partly correlate with the lower-crustal density variations. They also cross the basin segments in some areas. This could be an indication that the graben structures are overprinting older crustal blocks that can be identified from their lower-crustal densities. A few units do correlate. For example, the Yenissey anomaly that overlies the arch, and the mid-basin segment that trends SW–NE and is associated with rift-graben structures of the same orientation.

[46] The results of the gravity inversion also allow the distribution and thickness of basalts to be reinterpreted. The greatest thickness is found in the Pur Taz area and in the inferred graben structures. The Pur Taz area is characterized by three N–S to NW–SE trending linear structures in which the basalt layer thickens. One of these linear structures coincides with the Koltogory Urengoi structure and continues to the south where, after an initial reduction to almost zero thickness, it attains a thickness of up to 1.9 km in its southernmost part. Another interesting feature is the linear basalt thickness of up to 2.5 km in the proposed rift structure to the west of the Agan rift. This rift structure, previously proposed by *Allen et al.* [2006], is also clearly evident in the magnetic anomalies (Figures 3b and 9). In contrast, when considering the Khudottei rift, we find a disagreement with the interpretation of *Pavlov* [1995]. According to our inversion, a basalt thickness of up to 2.5 km is located west of the Khudottei rift proposed by *Pavlov* [1995]. At the supposed location of the Khudottei rift, no basalt thickening is found, and the gravity and magnetic fields also show no prominent anomalies. Therefore we propose that the Khudottei rift lies 100 km west of the location inferred by *Pavlov* [1995].

[47] In the magnetic anomaly map (Figure 3b), adjacent linear positive and negative anomalies are evident in the central part of the basin. The positive magnetic anomalies partly correlate with positive gravity anomalies. Given the high density and susceptibility of basalt with respect to sediment, these positive anomalies are presumably related to the partially basalt-filled buried rifts (Figure 9).

[48] Further study should incorporate a detailed analysis of the magnetic field because it has the potential to give a better estimate of the overall basalt volume. Combined interpretation of gravity and magnetic data provides a means to improve the interpretation of the sub-basalt sedimentary thickness [e.g., *Smallwood et al.*, 2001; *Reynisson et al.*, 2009], but the resolution of the magnetic data currently available for the West Siberian Basin does not allow such a detailed analysis.

[49] Our new picture of the crustal structure of the West Siberian Basin and, in particular, the interpretation of the presence of increased lower-crustal density has implications for the formation of the basin. The classical model of basin subsidence is the McKenzie rift model [*Allen and Allen*, 2005; *Lobkovsky et al.*, 1996; *McKenzie*, 1978] in which subsidence is an isostatic response to the post-rift cooling of the crust. However, *Stel et al.* [1993] have shown that the presence of increased density in the lower crust can act as a load on the base of the crust that increases the amount of space for sedimentation. The increased lower-crustal densities that we infer for the West Siberian Basin contribute a load of a few tens of MPa that adds to the load induced by cooling-induced densification. Neglecting this extra load would result in an overestimate of the load due to cooling alone, an overestimate of the cooling rate itself and an incorrect determination of the stretching factor. Therefore the existence of increased lower-crustal density may be an essential part of intracratonic basin formation.

[50] The presence of increased lower-crustal density may be a common feature of large-scale cratonic and intracratonic basins [*Braitenberg and Ebbing*, 2007, 2009]. Increased lower-crustal density has also been inferred for other basins such as the Michigan [*Nunn and Sleep*, 1984], Amazon [*Nunn and Aires*, 1988] and Barents Sea basins [*Ebbing et al.*, 2007]. The presence of increased densities in the lower crust can be explained as the combined effect of magmatic intrusion, partial melting of metamorphic rocks and removal of buoyant anatectic melts. The resulting density is intermediate to the underlying mantle and the overlying, less-dense crustal layers [*Sinigoi et al.*, 1995].

8. Conclusion

[51] We have used gravity and magnetic data to characterize the crustal structure of the West Siberian Basin. We used a gravity-field model derived from the integration of GRACE satellite data with terrestrial data [*Förste et al.*,

2008; *Tapley et al.*, 2004]. The use of the satellite-derived gravity field guarantees a uniform coverage of the basin and its surrounding areas.

[52] Correcting the gravity field for the effect of sedimentary layers and crustal thickness variations is essential for this study. Calculating the gravity effect of topography and crustal thickness is straightforward when a laterally constant density is assumed. The correction for the gravity effect of the sediments requires more effort because the density increase with depth has to be considered. For this purpose, we have used well constraints on horizon depths and two-way traveltime to invert for variations in velocity with depth. Empirical velocity-density relationships were then used to estimate the density variations with depth.

[53] The calculated residual gravity field is systematically positive and reflects the presence of unknown masses. We have attributed the positive residual gravity to increased density in the lower crust, most notably along the western (Urals) and eastern (Siberian craton) margins of the basin, as well as across the middle parts of the basin with a NE–SW orientation.

[54] The increased density partly underlies rift structures in the upper crust that extend for over 1500 km. We interpret the rifts to be partly filled with basalt that is up to 5 km thick. Our model of basalt thickness, although at present preliminary, could be used in combination with knowledge of the geochemical composition of basalts to estimate the total carbon dioxide and sulfur emitted during the extrusion of the West Siberian basalts. The amount of emitted volatiles is an essential input into discussions on the end-Permian mass extinction.

[55] The Koltogory-Urengoi rift that extends southward across the entire basin, has previously been described as the most evident structure in the basin [e.g., *Nikishin et al.*, 2002]. The gravity data suggest that a linear structure, extending over a length comparable, or even greater than, that of the Koltogory-Urengoi rift, is located along the eastern border of the basin. From the southern end of the basin it extends for over 1500 km before bending eastward into the Yenisey-Khatanga trough.

[56] Our results demonstrate the usefulness of global satellite-derived gravity data in the study of geologically interesting areas. The approach we have used can be applied in the same way to other areas without the geographical restrictions often imposed by the availability of terrestrial gravity data.

[57] **Acknowledgments.** We thank Ildiko' Nagy for her assistance in the bibliographic search and retrieval of documents, Stephanie Werner for assistance with the magnetic data retrieval, and Laura Marello for providing her study on density-velocity relationships. Hans Morten Bjørnseth, Christine Fichler, and Øyvind Steen from Statoil initiated our study and supplied us with information on the West Siberian Basin. We appreciate the assistance and help from all these people and especially StatoilHydro for funding our study. We are thankful to Ron Hackney and the associate editor, Allegra Hosford Scheirer, for comments that helped to significantly improve the quality of our manuscript. Great thanks to Ron Hackney for meticulous suggestions on the use of the English language. We acknowledge the use of the GMT mapping software by *Wessel and Smith* [1998].

References

Aleinikov, A. L., O. V. Bellavin, Yu. P. Bulasevich, I. F. Tavrin, E. M. Maksimov, M. Ya. Rudkevich, V. D. Nativkin, N. V. Shablinskaya, and V. S. Surkov (1980), Dynamics of the Russian and West Siberian Platforms, in *Dynamics of Plate Interiors*, edited by A. W. Bally, pp. 53–71, AGU, Washington, D. C.

Allen, P. A., and J. R. Allen (2005), *Basin Analysis: Principles and Applications*, 2nd ed., 549 pp., Blackwell Scientific Pub., Oxford, U. K.

Allen, M. B., L. Anderson, R. C. Searle, and M. Buslov (2006), Oblique rift geometry of the West Siberian Basin: Tectonic setting for the Siberian flood basalts, *J. Geol. Soc. London*, *163*, 901–904.

Artyushkov, E. V., and M. A. Baer (1986), Mechanism of formation of hydrocarbon basins: The West Siberia, Volga-Urals, Timan-Pechora basins and the Permian basin of Texas, *Tectonophysics*, *122*, 247–281.

Blakely, R. J. (1995), *Potential Theory in Gravity and Magnetic Applications*, 441 pp., Cambridge Univ. Press, New York.

Braitenberg, C., and J. Ebbing (2007), The gravity potential derivatives as a means to classify the Barents sea basin in the context of cratonic basins (extended abstracts), EGM 2007 International Workshop, Innovation in EM, Grav and Mag Methods: A new Perspective for Exploration, Villa Orlandi, Capri, Italy, 15–18 April. (Available at http://www2.ogs.trieste.it/egm2007/)

Braitenberg, C., and J. Ebbing (2009), The GRACE-satellite gravity and geoid fields in analysing large scale, cratonic or intracratonic basins, *Geophys. Prospect.*, doi:10.1111/j.1365-2478.2009.00793.x, in press.

Braitenberg, C., S. Wienecke, and Y. Wang (2006), Basement structures from satellite-derived gravity field: South China Sea ridge, *J. Geophys. Res.*, *111*, B05407, doi:10.1029/2005JB003938.

Braitenberg, C., S. Wienecke, J. Ebbing, W. Born, and T. Redfield (2007), Joint gravity and isostatic analysis for basement studies—a novel tool (extended abstracts), in *EGM 2007 International Workshop, Innovation in EM, Grav and Mag Methods: A New Perspective for Exploration*, Villa Orlandi, Capri, Italy, 15–18 April. (Available at http://www2.ogs.trieste.it/egm2007/)

Brocher, T. M. (2005), Empirical relations between elastic wavespeeds and density in the Earth's crust, *Bull. Seismol. Soc. Am.*, *95*, 2081–2092.

Czamanske, G. K., V. Gurevitch, V. Fedorenko, and O. Simonov (1998), Demise of the Siberian plume: Palaeogeographic and palaeotectonic reconstruction from the prevolcanic and volcanic record, north-central Siberia, *Int. Geol. Rev.*, *40*, 95–115.

Döring, J., and H.-J. Götze (1999), The isostatic state of the southern Urals crust, *Geol. Rundsch.*, *87*, 500–510.

Döring, J., H.-J. Götze, and M. Kaban (1997), Preliminary study of the gravity field of the southern Urals along the URSEIS '95 seismic profile, in *EUROPROBE's Uralides Project*, edited by A. Peres-Estaún, D. Brown, and D. Gee, *Tectonophysics*, *276*(1–4), 49–62, doi:10.1016/S0040-1951(97)00047-4.

Dziewonski, A. M., and D. L. Anderson (1981), Preliminary reference earth model, *Phys. Earth Planet. Inter.*, *25*, 297–356.

Ebbing, J., C. Braitenberg, and S. Wienecke (2007), Insights into the lithospheric structure and the tectonic setting of the Barents Sea region by isostatic considerations, *Geophys. J. Int.*, *171*, 1390–1403, doi:10.1111/j.1365-246X.2007.03602.x.

Forsberg, R. (1984), A Study of Terrain Reductions, Density Anomalies and Geophysical Inversion Methods in Gravity Field Modelling, *Reports of the Department of Geodetic Science and Surveying, No. 355*, Ohio State Univ., Columbus, Ohio.

Förste, C., et al. (2008), The GeoForschungsZentrum Potsdam/Groupe de Recherche de Geodesie Spatiale satellite-only and combined gravity field models: EIGEN-GL04S1 and EIGEN-GL04C, *J. Geod.*, doi:10.1007/s00190-007-0183-8.

Friberg, M., C. Juhlin, A. G. Green, H. Horstmeyer, J. Roth, A. Rybalka, and M. Bliznetsov (2000), Europrobe seismic reflection profiling across the eastern Middle Urals and West Siberian Basin, *Terra Nova*, *12*, 252–257.

Gardner, G. H. F., L. W. Gardner, and A. R. Gregory (1974), Formation velocity and density—the diagnostic basics for stratigraphic traps, *Geophysics*, *39*, 770–780.

Jones, E. J. W. (1999), *Marine Geophysics*, 466 pp., John Wiley, New York.

Karus, E. V., G. A. Gabrielyants, V. M. Kovylin, and N. M. Chernyshev (1984), Depth pattern of West Siberia, *Sov. Geol.*, *5*, 75–84, (in Russian).

Kovylin, V. M. (1985), Fault-block structure of the West Siberian Craton and its petroleum potential, *Sov. Geol.*, *2*, 77–86, (in Russian).

Lane, N. (2007), Mass extinctions—reading the book of death, *Nature*, *448*, 122–125.

Larsen, H. C., A. D. Saunders, P. D. Clift, and the Shipboard Scientific Party (1994), *Proceedings of the Drilling Programme Initial Report*, vol. 152, p. 86, Ocean Drill. Program. College Station, Texas.

Lobkovsky, L. I., et al. (1996), Extensional basins of the former Soviet Union—structure, basin formation mechanisms and subsidence history, *Tectonophysics*, *266*, 251–285.

Ludwig, W. J., J. E. Nafe, and C. L. Drake (1970), Seismic refraction, in *The Sea*, edited by A. E. Maxwell, vol. 4, part 1, pp. 53–84, Wiley-Interscience, New York.

McKenzie, D. (1978), Some remarks on the development of sedimentary basins, *Earth Planet. Sci. Lett.*, *40*, 25–32.

Morozova, E. A., I. B. Morozov, S. B. Smithson, and L. N. Solodilov (1999), Heterogeneity of the uppermost mantle beneath Russian Eurasia from the ultra-long-range profile QUARTZ, *J. Geophys. Res.*, *104*(B9), 20,329–20,348.

Mussett, A. E., and M. A. Khan (2000), *Looking Into the Earth. An introduction to Geological Geophysics*, 470 pp., Cambridge Univ. Press, Cambridge, U. K.

National Geophysical Data Center (1997), *Magnetic Anomaly Data of the Former USSR* [CD-ROM], Natl. Geophys. Data Cent., Boulder, Colo.

Nikishin, A. M., P. A. Ziegler, D. Abbott, M.-F. Brunet, and S. Cloetingh (2002), Permo–Triassic intraplate magmatism and rifting in Eurasia. Implications for mantle plumes and mantle dynamics, *Tectonophysics*, *351*, 3–39.

Nunn, J. A., and J. R. Aires (1988), Gravity anomalies and flexure of the lithosphere at the middle Amazon basin, Brazil, *J. Geophys. Res.*, *93*, 415–428.

Nunn, J. A., and N. H. Sleep (1984), Thermal contraction and flexure of intracratonal basins: A three-dimensional study of the Michigan basin, *Geophys. J. R. Astron. Soc.*, *76*, 587–635.

Peterson, J. A., and J. W. Clarke (1991), Geology and Hydrocarbon Habitat of the West Siberian Basin, *AAPG Studies in Geology # 32*, p. 96, AAPG, Tulsa, Okla.

Pavlov, Y. A. (1995), On recognition of rift structures in the basement of the West Siberian plate, *Geotectonics*, English Transl. (AGU), *29*(3), 213–223.

Pavlenkova, G. A., K. Priestley, and J. Cipar (2002), 2D model of the crust and uppermost mantle along rift profile, Siberian craton, *Tectonophysics*, *355*, 171–186.

Reynisson, R. F., J. Ebbing, and J. R. Skilbrei (2009), On the use of potential field data in revealing the basement structure in sub-basaltic settings. An example from the Møre margin offshore Norway, *Geophys. Prospect.*, doi:10.1111/j.1365-2478.2009.00795.x, in press.

Reichow, M. K., A. D. Saunders, R. V. White, M. S. Pringle, A. I. Al'Mukhamedov, A. Ya. Medvedev, and N. P. Kirda (2002), 40Ar/39Ar dates from the West Siberian Basin: Siberian Flood Basalt Province doubled, *Science*, *296*, 1846–1849.

Saunders, A. D., R. W. England, M. K. Reichow, and R. V. White (2005), A mantle plume origin for the Siberian traps: Uplift and extension in the West Siberian Basin, Russia, *Lithos*, *79*, 407–424.

Schissel, D., and R. Smail (2001), Deep mantle plumes and ore deposits, in *Mantle Plumes: Their Identification Through Time*, edited by R. E. Ernst and K. L. Buchan, *Geol. Soc. Am., Spec. Pap.*, *352*, 291–321.

Sengor, A. M. C., and B. A. Natal'in (1996), Paleotectonics of Asia: Fragments of a synthesis, in *The Tectonic Evolution of Asia*, edited by A. Yin and T. M. Harrison, pp. 486–641, Cambridge Univ. Press, New York.

Shin, Y. H., H. Xu, C. Braitenberg, J. Fang, and Y. Wang (2007), Moho undulations beneath Tibet from GRACE-integrated gravity data, *Geophys. J. Int.*, 1–15, doi:10.1111/j.1365-246X.2007.03457.x.

Sinigoi, S., J. E. Quick, A. Mayer, and G. Demarchi (1995), Density-controlled assimilation of underplated crust, Ivrea-Verbano zone, Italy, *Earth Planet. Sci. Lett.*, *129*, 183–191.

Smallwood, J. R., M. J. Towns, and R. S. White (2001), The structure of the Faeroe-Shetland Trough from integrated deep seismic and potential field modelling, *J. Geol. Soc.*, *158*, 409–412.

Stel, H., S. Cloetingh, M. Heeremans, and P. van der Beck (1993), Anorogenic granites, magmatic underplating and the origin of intracratonic basins in a non-extensional setting, *Tectonophysics*, *226*, 285–299.

Surkov, V. S. (2002), Neogean evolution of the young Ural–Siberian platform, *Geol. Geofiz.*, *43*, 754–761.

Surkov, V. S., A. A. Trofimchuk, O. G. Zhero, A. E. Kontorovich, and L. V. Smirnov (1982), The Triassic rift system of the West Siberian plate and its influence on the hydrocarbon potential of the Mesozoic-Cenozoic platform cover, *Geol. Geofiz.*, *8*, 3–15.

Surkov, V. S., V. P. Devyatov, O. G. Zhero, A. M. Kazakov, V. N. Kramnik, and L. V. Smirnov (1993), The Earth's crust structure in the region of the Tyumen' superdeep borehole, *Geol. Geofiz.*, *1*, 120–126.

Tapley, B., S. Bettadpur, M. Watkins, and C. Reigber (2004), The gravity recovery and climate experiment: Mission overview and early results, *Geophys. Res. Lett.*, *31*, L09607, doi:10.1029/2004GL019920.

Tscherning, C. C., R. Forsberg, and P. Knudsen (1992), The GRAVSOFT package for geoid determination, in *Proc. 1. Continental Workshop on the Geoid in Europe, Prague, May 1992*, pp. 327–334, Res. Inst. of Geod., Topogr. and Cartogr., Prague.

Ulmishek, G. (2003), Petroleum geology and resources of the West Siberian Basin, Russia, *U.S. Geol. Surv. Bull. 2201-G*, 49 pp. (Available at http://pubs.usgs. gov/bul/2201/G/)

Vyssotski, A.V., V. N. Vyssotski, and A. A. Nezhdanov (2006), Evolution of the West Siberian Basin, *Mar. Pet. Geol.*, *23*, 93–126.

Wessel, P., and W. H. F. Smith (1998), New, improved version of generic mapping tools released, *Eos Trans. AGU*, *79*(47), 579.

C. Braitenberg, Department of Earth Sciences, University of Trieste, Via Weiss 1, I-34100 Trieste, Italy. (berg@units.it)

J. Ebbing, Geological Survey of Norway, Leiv Eirikssons vei 39, N-7491 Trondheim, Norway. (joerg.ebbing@ngu.no)